American Mineralogist, Volume 97, pages 1177–1186, 2012

A first-principle investigation of antigorite up to 30 GPa: Structural behavior under compression

Gian Carlo Capitani[1,*] and Lars Stixrude[2]

[1]Dipartmento di Scienze Geologiche e Geotecnologie, Università di Milano Bicocca, P.za della Scienza 4, 20126 Milano, Italy
[2]Department of Earth Sciences, University College London, Gower Street, London WC1E 6BT, U.K.

Abstract

The structure of antigorite (m = 17) has been studied by density functional theory from 0 to 30 GPa. The fourth-order Birch-Murnaghan equation of state fit of the thermally corrected LDA results yields an equilibrium volume (V_0 = 2853.13 Å^3), bulk modulus (K_0 = 64.6 GPa), and its pressure derivative (K_0' = 6.94) in good agreement with experimental results. Two changes in compression mechanism occur at 6.1 and 20.5 GPa, individuating three pressure ranges: (1) in the low-pressure range, the antigorite wave flattens and the interlayer thickness decreases rapidly; (2) in the intermediate-pressure range, in-plane rotations of tetrahedra (ditrigonalization) and then wave-bending become the dominant compression mechanisms; (3) in the extreme-pressure range, the mechanism of wave-bending becomes prevalent. The first change reveals the origin of softening found experimentally near 6 GPa: the change in compression mechanism occurs after the minimal mismatch between T- and O-sheets is achieved and is accompanied by an apparent symmetry breaking: accidental degeneracies of structural parameters between short and long halfwaves are lifted, including T-sheet thicknesses and Si-O bond lengths. In the extreme-pressure range, Si-O-Si angles decrease below 122°, which may be the origin of amorphization found experimentally at similar pressure.

Keywords: Antigorite, first principles, equation of state, structure

Introduction

Containing up to 12–13% water and stable to depths of perhaps 150–200 km in very cold subducting slabs, antigorite is the most hydrated mineral subducted into the mantle. Its dehydration may be one major cause for mantle wedge hydration and partial melting processes (Ulmer and Trommsdorff 1995; Tonarini et al. 2007), as well as for deep focus earthquakes (Peacock 2001; Dobson et al. 2002; Yamasaki and Seno 2003).

Antigorite is a 1:1 sheet silicate of the serpentine group, with ideal formula $Mg_3Si_2O_5(OH)_4$. It forms a wavy structure in which the tetrahedral sheet switches polarity periodically. It is structurally related to lizardite, the flat serpentine polymorph, and chrysotile, which forms cylindrical tubes (Wicks and O'Hanley 1988). While lizardite and chrysotile forms pseudomorphic textures after hydrothermal alteration of olivine and pyroxenes, antigorite is considered the prograde serpentine mineral, stable up to 600–700 °C and 6–7 GPa (Bose and Ganguly 1995; Ulmer and Trommsdorff 1995; Wunder and Schreyer 1997). However, the reasons accounting for the different serpentine stability fields are not yet understood, and the origin of the structural corrugation is still matter of debate.

Because of its geological relevance, antigorite has been investigated under high-pressure conditions in the diamond-anvil cell (DAC) by Raman (Auzende et al. 2004; Reynard and Wunder 2006) and infrared (IR) (Noguchi et al. 2012) spectroscopy; powder (Irifune et al. 1996; Hilairet et al. 2006a), and single-crystal (Nestola et al. 2009) X-ray diffraction (XRPD and SCXRD, respectively). Most of these studies find changes in the compression behavior at 6 GPa. However, the origin of this change in behavior is still unclear because recurrent structural defects affecting antigorite (e.g. Capitani and Mellini 2005), and the reduced data set resulting from a DAC experiment—the reciprocal space is partially hidden by the DAC apparatus—frustrate structure refinement.

In this work, we overcome the experimental difficulties by exploiting theoretical methods based on density functional theory (DFT) to simulate the structural evolution of antigorite m = 17 under compression. The method has already been successfully employed on antigorite to complement biased experimental results (Capitani et al. 2009) and for elasticity (Mookherjee and Capitani 2011). To gain additional insight into the compression mechanism and pressure-induced amorphization, we have extended the study of antigorite well beyond its presumed thermodynamic stability limit, up to a pressure of ~30 GPa. Results, including the predicted equation of state, lattice parameters, and internal structure parameters, reveal two changes in compression mechanism. Among these are mechanisms not previously recognized in silicates, such as wave-bending, that are important for understanding experimentally observed softening anomalies and the behavior of antigorite in Earth's interior.

Methods

Static calculations were performed with the planewave pseudopotential method (Heine 1970) as implemented in the Vienna ab initio simulation package (VASP) (Kresse and Hafner 1993; Kresse and Furthmüller 1996a, 1996b), using ultrasoft Vanderbilt-type (Vanderbilt 1990; Kresse et al. 1992) pseudopotentials. We present results in the local density (LDA) and generalized gradient (GGA)

* E-mail: giancarlo.capitani@unimib.it

0003-004X/12/0007–1177$05.00/DOI: http://dx.doi.org/10.2138/am.2012.3956

approximations (Lundqvist and March 1983; Perdew et al. 1996), focusing on the former as these yield superior agreement with experimental data.

The antigorite m = 17 polysome, monoclinic (Pm), with 194 atoms in the asymmetric unit (291 in the cell), is one of the most complex crystalline Earth materials ever studied at high pressure with theoretical methods. Room-pressure optimized structures from our previous results (Capitani et al. 2009) were used as an initial guess for further structural relaxations at compressed volumes (3000, 2900, 2800, 2700, 2600, 2500, 2400, 2300, and 2200 Å^3). The structural relaxation scheme (Wentzcovitch 1991; Wentzcovitch et al. 1993) conserves the space group symmetry. All computations were performed in the primitive unit cell [291 atoms, i.e., one unit formula of $Mg_{48}Si_{34}O_{85}(OH)_{62}$]. We used an energy cutoff of 500 eV, and a Monkhorst-Pack (Monkhorst and Pack 1976) 1 × 2 × 2 k-point mesh. Convergence tests with respect to the basis set size and Brillouin zone sampling were carried out at 600 eV cutoff on the basis set and 2 × 2 × 2 k-point grid, yielding total energies and pressures that are converged within 0.6 meV/atom and 0.4 GPa, respectively.

Static calculations do not include the effects of lattice vibrations. To compare our results more directly with room-temperature experiment, we use a Debye-Grüneisen model (Ita and Stixrude 1992):

$$P(V,T) = P_{\text{static}}(V) + \frac{\gamma}{V}\left[(E_{\text{ZP}}(V) + E_{\text{TH}}(V,T)\right] \quad (1)$$

where P_{static} is the static pressure calculated from DFT, V is the volume of the unit cell, γ the Grüneisen parameter, and E_{ZP} and E_{TH} are the energies due to zero-point motion and the thermal energy at 300 K, respectively, which depend on the Debye temperature θ_D (Panero and Stixrude 2004):

$$E_{\text{ZP}} = \frac{9nk_{\text{B}}\theta_{\text{D}}}{8} \quad (2)$$

$$E_{\text{TH}} = 9nk_{\text{B}}T\left(T/\theta_{\text{D}}\right)^3 \int_0^{\theta_D/T} \frac{x^3}{e^x - 1}dx \quad (3)$$

where n is the number of atoms in the unit cell (291) and k_B is the Boltzman constant ($1.38 \cdot 10^{23}$ J/K). Given the similarity of the antigorite structure with that of lizardite, we employed the same values of θ_D = 830 K and γ = 0.68, successfully tested for lizardite by Mookherjee and Stixrude (2009).

Our results were fit with the Birch-Murnaghan (Birch 1947) equation of state, which is based upon the Eulerian finite strain:

$$f_E = \frac{1}{2}\left[\left(\frac{V_0}{V}\right)^{2/3} - 1\right]. \quad (4)$$

Expansion to the fourth order in the strain (BM4) gives:

$$P = 3K_0 f_E\left(1 + 2f_E\right)^{5/2}\left\{\begin{array}{l} 1 + \frac{3}{2}\left[K_0' - 4\right]f_E + \\ \frac{3}{2}\left[K_0K_0'' + \left(K_0' - 4\right)\left(K_0' - 3\right) + \frac{35}{9}\right]f_E^2 \end{array}\right\}. \quad (5)$$

A truncation to second order in energy (BM2), implies a fixed value of K_0' = 4 (higher-order terms are ignored). The third-order truncation (BM3) yields an implied value of K_0'' given by (Anderson 1995):

$$K_0'' = -\frac{1}{K_0}\left[\left(3 - K_0'\right)\left(4 - K_0'\right) + \frac{35}{9}\right]. \quad (6)$$

We determined the linear moduli (K_α) by fitting our theoretical lattice parameters as function of pressure, to linear finite strain expansions (Meade and Jeanloz 1990; Wentzcovitch and Stixrude 1997), assuming the compression to be pseudoorthogonal (Stixrude 2002):

$$F_\alpha = K_\alpha + m_\alpha \cdot f_\alpha \quad (7)$$

$$F_\alpha = \frac{P}{f_\alpha(1 + 2f_\alpha)(1 + 2f_E)} \quad (8)$$

where $\alpha = a$, b, $c\cdot\sin\beta$, are our determined lattice parameters as function of pressure, m_α is related to the pressure dependence of K_α, and f_α is the Eulerian finite strain defined as:

$$f_\alpha = \frac{1}{2}\left[\left(\frac{\alpha_0}{\alpha}\right)^2 - 1\right] \quad (9)$$

where α_0 is the lattice parameter at zero pressure.

RESULTS

Equation of state

Bulk compressibility. Unit-cell parameters and volumes are reported in Table 1. The predicted cell volume up to 30 GPa of antigorite m = 17 is shown in Figure 1, along with the experimental results on antigorite of Nestola et al. (2009), and the theoretical result on lizardite of Mookherjee and Stixrude (2009). LDA and GGA static results bracket the experimental result for antigorite.

The thermal correction leads to a zero-point motion contribution of ~0.9 GPa and to a thermal pressure contribution of ~0.3 GPa, for a total pressure correction to static results of ~1.2 GPa. Thermal corrections improve agreement between LDA and experiments and worsen that between GGA and experiments. Further discussion on the antigorite structural evolution at high pressure will focus on LDA results only, if not differently specified.

To fit the data, the third-order (BM3) and the fourth-order (BM4) Birch-Murnaghan EoS were tested, analyzing the relative F_E-f_E plots (inset Fig. 1). Here, F_E is the normalized stress defined as:

$$F_E = \frac{P}{3f_E(1 + 2f_E)^{5/2}}. \quad (10)$$

Strong curvature in F_E vs. f_E space shows the importance of including a fourth order term in the Eulerian finite strain expansion. Our finding that a third-order expansion is inadequate is consistent with that of Nestola et al. (2009), who however fit separate third EoS to low (P < 6 GPa) and high (P > 6 GPa) regimes. Instead we find that a fourth-order EoS can universally fit our results up to 30 GPa, a maximum pressure much greater than that achieved in the experiments.

The BM4 fit of thermally corrected LDA values yields V_0 = 2853.13 Å^3, K_0 = 64.55, and K_0' = 6.94, which compare nicely with V_0 = 2913.99 Å^3, K_0 = 62.9, and K_0' = 6.1 from SCXRD-DAC experiments (Nestola et al. 2009) and other DAC experiments (Hilairet et al. 2006a; Bezacier et al. 2010; Table 2). The small differences are probably due to the approximations to the exchange and correlation functional, and are similar in magnitude to that found in other DFT studies on sheet silicates, such as talc (Stixrude 2002) and lizardite (Mookherjee and Stixrude 2009). Deviations between theory and experiments may also arise from the fact that in the present work we considered a perfect crystal, free of defects such as b/3 stacking disorder—always present even in the most ordered antigorite so far reported, i.e., Mg159 Val Malenco specimens (Capitani and Mellini 2004, 2005)—and we did not consider the influence of Al and Fe substituent for Mg (and possibly Si), significant in the Almirez specimens (Padrón-Navarta et al. 2008) used in DAC experiments.

TABLE 1. Unit-cell parameters at different pressures and unit-cell volumes

V (Å^3)	3000	2922.326	2900	2800	2700	2600	2500	2400	2300	2200
P_{LDA}^{static} (GPa)	−3.64	−2.67	−2.30	−0.09	3.10	6.80	11.41	16.76	21.90	28.88
P_{LDA}^{300K} (GPa)	−2.46	−1.49	−1.12	1.09	4.28	7.98	12.59	17.94	23.08	30.06
a (Å)	43.5477	43.4049	43.3538	43.0688	42.6391	42.0698	41.4395	40.7481	39.9965	39.2680
b	9.2727	9.2428	9.2341	9.1750	9.0923	8.9947	8.8849	8.7693	8.6823	8.5837
c	7.4310	7.2858	7.2454	7.0871	6.9655	6.8713	6.7901	6.7165	6.6241	6.5305
β (°)	91.19	91.17	91.11	91.02	90.92	90.61	90.26	89.97	89.12	88.12
P_{GGA}^{static} (GPa)	0.65	2.18	2.70	5.66	9.53	13.58	18.76	23.43	29.39	36.95
P_{GGA}^{300K} (GPa)	1.83	3.36	3.88	6.84	10.71	14.76	19.94	24.61	30.58	38.14
a (Å)	43.7875	43.5974	43.5184	43.1098	42.6438	42.0237	41.4137	40.7168	39.9743	39.1933
b	9.3207	9.2786	9.2661	9.1884	9.0969	8.9902	8.8807	8.7948	8.7009	8.6063
c	7.3522	7.2255	7.1930	7.0700	6.9612	6.8822	6.7975	6.7028	6.6145	6.5270
β (°)	91.18	91.12	91.11	90.96	90.93	90.52	90.19	89.16	88.69	87.79

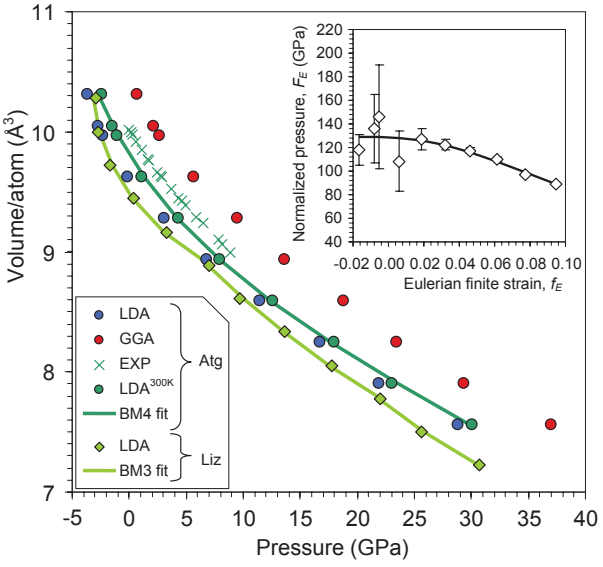

FIGURE 1. Unit-cell volume/atom vs. pressure for antigorite m = 17 (circles = this study; crosses = Nestola et al. 2009, experimental data) and lizardite (diamonds = Mookherjee and Stixrude 2009; BM3 fit over three distinct pressure ranges). The lower volume per atom of lizardite with respect to antigorite may originate from the slightly different formula unit, $Mg_3Si_2O_5(OH)_4$ and $Mg_{2.82}Si_2O_5(OH)_{3.65}$, respectively. This in turn is due to the local talc structure occurring at 6-reversals in antigorite (Capitani and Mellini 2004), which makes antigorite and lizardite not polymorphs in stricto sensu. Inset: F_E vs. f_E plots for antigorite (diamonds) and related BM4 fit (solid line). Error bars calculated assuming uncertainty in the pressure of ±0.3 GPa. (Color online.)

Linear compressibility. The theoretical axis lengths agree with those determined experimentally by Nestola et al. (2009) to within 0.7, 0.5, and 0.9% for a, b, and c, respectively. Their relative compressibility is significantly anisotropic, with the compression behavior changing with pressure. The c parameter is initially the most compressible and b the stiffest. Above ~6 GPa, however, the c parameter becomes abruptly stiffer and comparatively less compressible than a (Fig. 2). The latter, moreover, records an abrupt softening at ~20 GPa (inset Fig. 2).

Our predicted axial compressibilities have the ratio β_a:β_b:β_c = 1.09:1.00:2.45 (Table 3), nearly identical to that found in power X-ray diffraction experiments by Hilairet et al. (2006a) (1.11:1.00:2.48), while other experimental values show a relatively softer c-direction. Brillouin scattering shows b more compressible than a in disagreement with our findings, as well as with those on talc (Stixrude 2002). Our predicted linear compressibility appears similar with that of lizardite calculated with the same method, β_c:β_a = 2.78 (Mookherjee and Stixrude 2009), and with the theoretical results on antigorite elasticity of Mookherjee and Capitani (2011). Indeed, the compressibility along c in antigorite should be lower than in lizardite due to the presence of stiffer ionic bonds in the interlayer at reversal lines (Capitani and Mellini 2004, 2006). This seems confirmed, both experimentally and theoretically, also by the evolution of the along stacking compressibility with pressure (Fig. 2).

TABLE 2. Equilibrium volume and bulk compressibility of antigorite

	LDA	GGA	LDA	Experimental		
	BM4 static	BM4 static	BM4 300 K	XRPD*	SCXRD†	Brillouin‡
V_0 (Å^3)	2804.31	3012.31	2853.13	2926.23	2913.99	2924.64
K_0 (GPa)	72.33	71.94	64.55	67.27	62.90	60.80
K_0'	6.26	3.49	6.94	*4.00*	6.10	–
K_0'' (GPa^{-1})	−0.05	−0.08	−0.65	–	*−0.17*	–

Note: Implied values in italics.
* Hilairet et al. (2006a).
† Nestola et al. (2009).
‡ Bezacier et al. (2010).

Interpolyhedral structural readjustment

Ditrigonal distortion. Ditrigonal distortion is an important compression mechanism, particularly in the intermediate and extreme pressure ranges. Tetrahedrdal rotation allows the T-sheet to maintain registry with the O-sheet on compression, and occurs differently in the short and in the long halfwave and among reversal rings. In-plane rotation of tetrahedra is quantified by the average deviation of the tetrahedral rings (Fig. 3) from the perfect hexagonal configuration with an angle of 120° formed by triples of basal oxygen atoms:

$$2\alpha = \Sigma_i\langle|\phi_i - 120|\rangle \quad (11)$$

where ϕ_i is the angle formed by triples of basal oxygen atoms. 2α may assume values from 0 to 60°, the latter corresponding to the theoretical triangular shape, and it is labeled positive if the concerted tetrahedral movement brings the basal O atoms closer to the nearest octahedral atom and far away from the external hydroxyls, negative in the opposite case (Mellini 1982).

Our results show negative ditrigonal distortion and an increase in tetrahedral rotation with increasing pressure (Fig. 4; Supplementary Table 4[1]). A similar increase of the ditrigonal distortion with compression has been observed also in the modeled compression of lizardite (Mookherjee and Stixrude 2009)

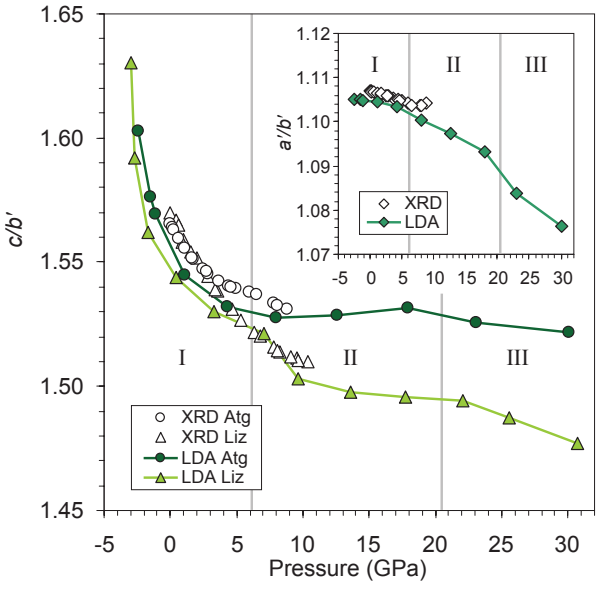

FIGURE 2. Along-stacking axial compressibility vs. pressure of antigorite (circles and diamonds) and lizardite (triangles). Filled symbols with trend lines = LDA results (Mookherjee and Stixrude 2009); empty symbols = experimental results (Hilairet et al. 2006a; Nestola et al 2009). Inset: in-layer axial compressibility of antigorite. To facilitate comparison, the *b* parameter of lizardite was recalculated as $b' = a \cdot \sqrt{3}/2$ (trigonal to monoclinic transformation); the *a* parameter of the $m = 17$ antigorite polysome as $a' = a/8.5$, and *b* as $b' = b/2$ (the lizardite subcell, Uehara and Shirozu 1985). The three pressure ranges individuated in this study are indicated by gray vertical lines. (Color online.)

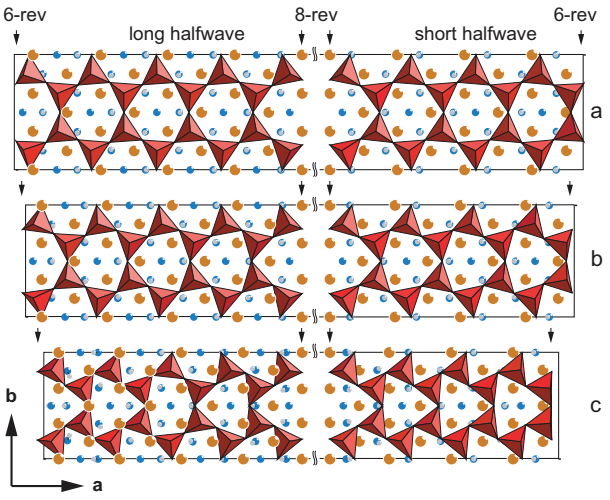

FIGURE 3. [001] projection of the antigorite m = 17 structure: (**a**) V = 3000 Å^3 (10.3 Å^3/atom; –2.5 GPa); (**b**) V = 2600 Å^3 (~8.9 Å^3/atom; 8 GPa); (**c**) V = 2200 Å^3 (7.6 Å^3/atom; 30 GPa). Red = SiO_4 tetrahedra; maroon = magnesium atoms; blue = O atoms; gray = hydrogen atoms. Arrows indicate positions of 6- and 8-reversals. Short halfwave (**right**) upside down. (Color online.)

and talc (Stixrude 2002). A sharp change in behavior is observed at ~6 GPa, where accidental degeneracies between short and long halfwaves are lifted and tetrahedral rotation begins to increase at a greater rate in the short halfwaves with further increase in pressure. Distinct trends also occur upon compression for the reversals. The 4-reversal shows three different slopes in three different pressure ranges: it remains almost constant up to ~6 GPa; increases abruptly from almost null values from 6 to 20 GPa; then more smoothly above 20 GPa. Tetrahedral rotation at the 4-reversal is less than that at other structural positions because of the higher silicon-silicon repulsive forces in the small rings that oppose rotation. Consistently, the 6-reversal increases rotation with increasing pressure at higher rate than 4-reversal. The 8-reversal, which is connected to the 4-reversal and thus in part constrained by it, assumes intermediate values. It is remarkable that in the short (even) halfwave the distortion affects evenly the hexagonal rings throughout the compression range investigated, whereas in the long (odd) halfwave there is a heterogeneous distribution of the ditrigonal distortion at high pressure (Fig. 3c).

TABLE 3. Axial compressibility and equilibrium cell parameters of antigorite

	DFT	EXP		
	LDA 300K	XRPD*	SCXRD†	Brillouin‡
a_0 (Å)	43.20	43.56	43.52	43.59
K_{a0} (GPa)	276.56	270.78	294.00	344.83
β_a (GPa^{-1})	0.0036	0.0037	0.0034	0.0029
b_0 (Å)	9.20	9.26	9.25	9.26
K_{b0} (GPa)	300.81	299.76	327.00	270.27
β_b (GPa^{-1})	0.0033	0.0033	0.0031	0.0037
c_0 (Å)	7.18	7.26	7.24	7.25
K_{c0} (GPa)	125.40	120.98	101.40	103.09
β_c (GPa^{-1})	0.0081	0.0083	0.0099	0.0097

* Hilairet et al. (2006a) (cell parameters from XRPD at ambient conditions).
† Nestola et al. (2009); linear moduli ×3 since the method they used yields values three times smaller than actual and not consistent with the relation $1/K_0 = 1/K_{a0} + 1/K_{b0} + 1/K_{c0}$. Compressibilities are also converted into standard positive values.
‡ Bezacier et al. (2010) (cell parameters from XRPD).

Curvature of the halfwaves. The bending of the waves is a second major compression mechanism in the intermediate pressure range and at elevated pressure when the linear compressibility along **a** exceeds that across the TO-layer. The curvature of the halfwaves reaches a minimum at ~6 GPa (Figs. 5 and 6 and Supplementary Table 5[1]). With increasing pressure, the curvature increases at different rate in the long and short halfwave, respectively. The difference is amplified beyond ~20 GPa when the trend of the short halfwave abruptly steepens, whereas that of the long halfwave plateaus. The distortion affects the short halfwave more than the long one.

Si-O-Si angle. The angle the bridging O atoms form with the linked silicon atoms decreases on compression and falls below the value 122° over the pressure range 22–28 GPa (Fig. 7 and Supplementary Table 6[1]). This critical value of the Si-O-Si angle has been identified as a measure of structural instability (e.g., Stixrude 2002). Silicates at ambient conditions show Si-O-Si angles larger than 122° (O'Keeffe and Hyde 1978). The average Si-O-Si angle shows a quick decrease with increasing

[1] Deposit item AM-12-048, Supplementary Tables 4–9. Deposit items are available two ways: For a paper copy contact the Business Office of the Mineralogical Society of America (see inside front cover of recent issue) for price information. For an electronic copy visit the MSA web site at http://www.minsocam.org, go to the *American Mineralogist* Contents, find the table of contents for the specific volume/issue wanted, and then click on the deposit link there.

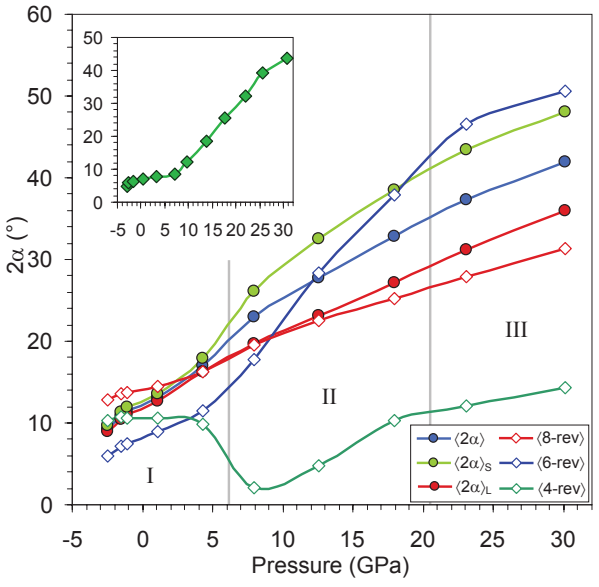

FIGURE 4. Ditrigonal distortion vs. pressure for antigorite m = 17 (this study) and lizardite (Mookherjee and Stixrude 2009, inset). $2\alpha = \Sigma_{i=6}|\varphi - 120°|/6$ for 6-membered rings, included the 6-reversal (6-rev); $2\alpha = \Sigma_{i=8}|\varphi - 135°|/8$ for 8-reversal (8-rev); $2\alpha = \Sigma_{i=4}|\varphi - 90°|/4$ for 4-reversal (4-rev). L = long halfwave; S = short halfwave. The three pressure ranges individuated in this study are indicated by gray vertical lines. (Color online.)

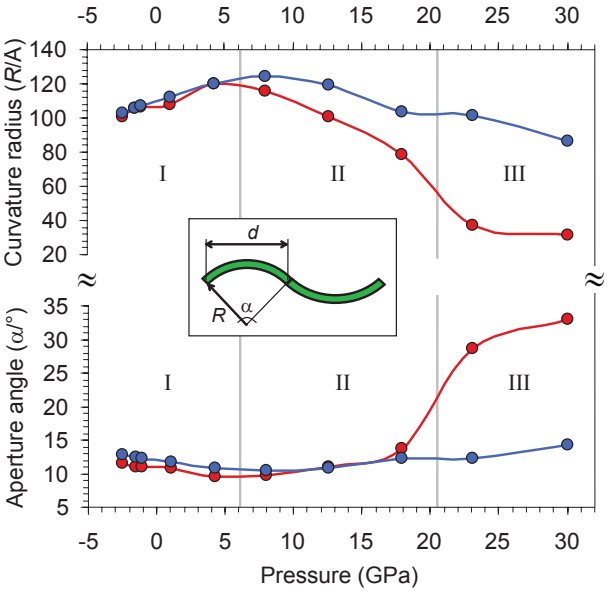

FIGURE 5. Halfwaves' radius of curvature and aperture angle vs. pressure (blue circle = long halfwave; red circle = short halfwave). Inset: schematic for the definition of the aperture angle (α), radius of curvature (R), and halfwave length (d). (Color online.)

pressure and, as for other structural parameters, from ~6 GPa onward it decreases at different rates in the short and long halfwave, respectively, appearing as symmetry breaking (Fig. 7; Supplementary Table 6).

Intrapolyhedral structural readjustment

Mg-O and Si-O bonds. The Si-polyhedra are stiffer and more regular than the Mg-polyhedra over the entire pressure range investigated, as in many other silicates (Fig. 8; Supplementary Table 7[1]). External Mg-O_W distances (Mg ligands on the side of the interlayer) are always distinctly and constantly shorter than internal Mg-O_V distances (toward the T-sheet). The Si-O_A bonds (bonds with the apical O atoms) are consistently shorter than the Si-O_B bonds (bonds with the basal O atoms) as in other sheet silicates (Stixrude 2002). At ~6 GPa an accidental degeneracy is lifted and Si-O_B distances in long and short halfwaves diverge: with the Si-O_B bonds of the long halfwave becoming more compressible than those in the short halfwave. That entails a higher average distortion of tetrahedra in the short halfwave than in the long one.

O- and T-sheet thickness. The average thickness of the O-sheet decreases slightly from negative pressures to ~6 GPa, then increases moderately up to the highest pressure investigated (Fig. 9, Supplementary Table 8[1]). In contrast, as for the Si-O bonds, a striking discontinuity affects the evolution with pressure of the average T-sheet thickness and T-base distance (distance of the silicon atom to the basal oxygen plane) at 6 GPa. From this value of pressure onward, these crystallographic parameters contract in the short halfwave at higher rate than in the long one, appearing, to be symmetry breaking.

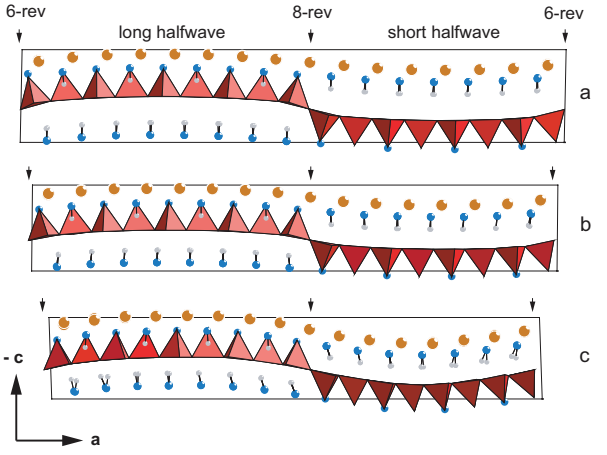

FIGURE 6. [010] projection of the calculated antigorite m =17 structure: (**a**) V = 3000 Å^3; (**b**) V = 2600 Å^3; (**c**) V = 2200 Å^3 (symbols as in Fig. 3). (Color online.)

The higher polyhedral distortion affecting the tetrahedra, in particular in the short halfwave, is also confirmed by classical distortion parameters such as the angle variance (a measure of the deviation of the intrapolyhedral bond angles from the ideal polyhedron) and the quadratic elongation (a measure of the deviation of bond lengths from the ideal polyhedron; Robinson et al. 1971): both decrease with increasing pressure in the O-sheet (that becomes more regular) and both increase with increasing pressure in the T-sheet (that becomes more distorted; Supplementary Table 9[1]), as observed also in lizardite (Mookherjee and Stixrude 2009) and talc (Stixrude 2002). Globally, the T- and O-sheets converge toward common distortion values at 30 GPa.

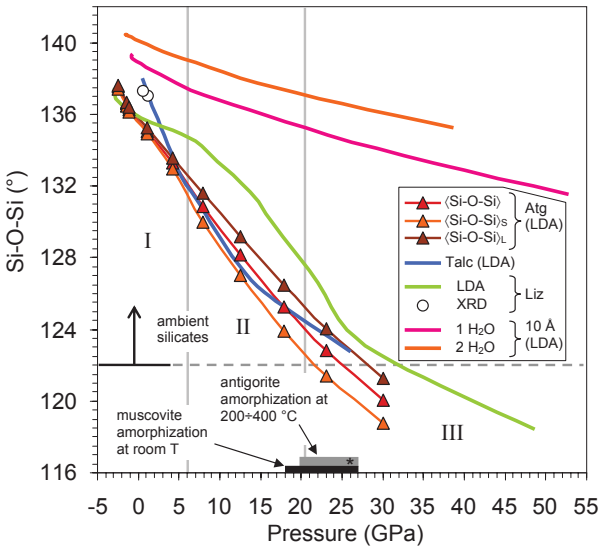

FIGURE 7. Average Si-O-Si angle vs. pressure of antigorite $m = 17$ (S = short halfwave; L = long halfwave). For comparison we report also: Si-O-Si angles observed in silicates at ambient conditions (O'Keeffe and Hyde 1978); Si-O-Si angles vs. pressure for in talc (Stixrude 2002); lizardite, both experimental (Mellini and Zanazzi 1987) and theoretical (Mookherjee and Stixrude 2009); and 10 Å phase, for one water molecule and two water molecules, respectively (Fumagalli and Stixrude 2007); the range of pressure over which muscovite becomes amorphous (Faust and Knittle 1994); the range of pressure over which antigorite becomes amorphous at temperatures between 200 and 400 °C (Irifune et al. 1996) and at 300 °C (Noguchi et al. 2012, star). (Color online.)

Hydrogen bonding

Bonds and angles across the interlayer. Hydrogen bonding in antigorite is weak or absent as shown by the evolution of hydrogen bond length parameters on compression (Fig. 10). While O-H bond lengths increase slightly on compression in the low-pressure regime, they decrease on compression at higher pressure. The trend of O-H vs. O···O distances do not conform to the expectations of hydrogen bonding as seen in ice, or other high-pressure phases such as AlOOH where hydrogen bonding is strong (Fig. 11). On the contrary, our results indicate weak hydrogen bonding in antigorite at volumes near the theoretically determined equilibrium volume, and lack of hydrogen bonding enhancement with compression, in agreement with the high-pressure Raman experiments of Auzende et al. (2004) and Reynard and Wunder (2006), on natural and synthetic antigorite samples, respectively, and with the infrared spectroscopy experiments of Noguchi et al. (2012).

O-H vector direction. The angle the O-H vector makes with the (001) normal is defined positive if pointing outwardly with respect the center of the ditrigon, negative if pointing toward the center of the ditrigon (Mookherjee and Stixrude 2009). The O-H vector "flips" with a change in sign of the angle on compression in lizardite with various structural consequences. In antigorite, the same change in sign occurs, but over a range of pressure (Fig. 12). Antigorite is different in this respect from lizardite because in the flat structure only one O-H bond environment occurs, whereas in antigorite there are a large variety of O-H bond environments and each of these changes the sign of the angle at a different value of the compression.

In the modeled compression of antigorite, the O-H vector angles are positive and hydrogens interact with the bridging basal O atoms forming the wider angle of the ditrigonal rings (Fig. 12; see also Fig. 3a). Upon compression, the O-H vector angles decrease, and at ~20 GPa (V/atom < 8.1 Å^3) the average becomes negative. At extreme conditions, the oxygen atoms interacting with the hydroxyls are now either basal O atoms forming the wider angle of the ditrigonal rings (the large majority), or those forming the narrower angle (mostly located in the long halfwave; Fig. 3c). The latter is the only configuration found in lizardite (cf. Fig. 2c of Mookherjee and Stixrude 2009).

The flipping of the O-H vector direction at ~20 GPa (see also Fig. 6) is paralleled by a steeper decrease of the O_W-H···O_B angle across the interlayer (Fig. 10). Although the flipping of the O-H vector occurs at roughly the same pressure in lizardite (22 GPa), the O-H···O angle in this case plateaus and the hydroxyl changes their interaction environment with the tetrahedral O atoms, which eventually leads to a vanishing of the tetrahedral bulk modulus and a collapse of the interlayer, a phenomenon not observed in antigorite.

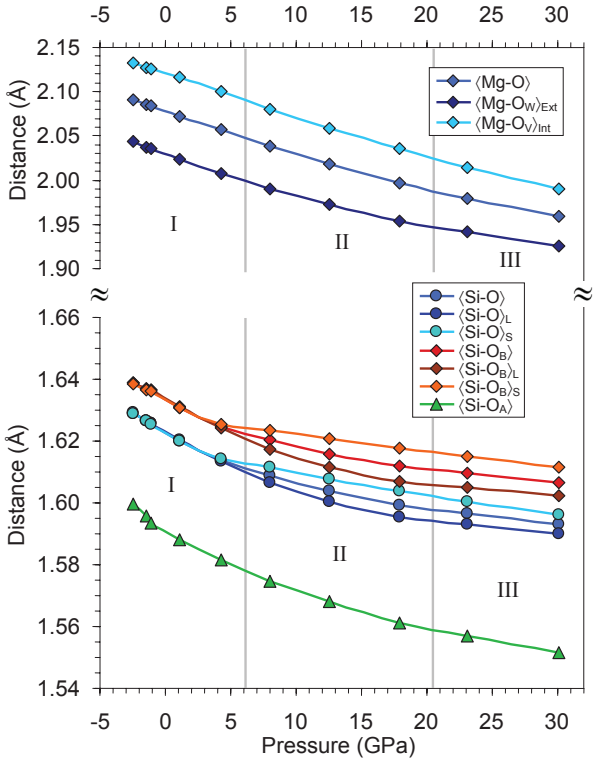

FIGURE 8. Average Mg-O bond and Si-O bond distances vs. pressure (Ext: external O atoms; Int: internal O atoms; A = apical O atoms; B = basal O atoms; L = long halfwave; S = short halfwave). The three pressure ranges individuated in this study are indicated by gray vertical lines. (Color online.)

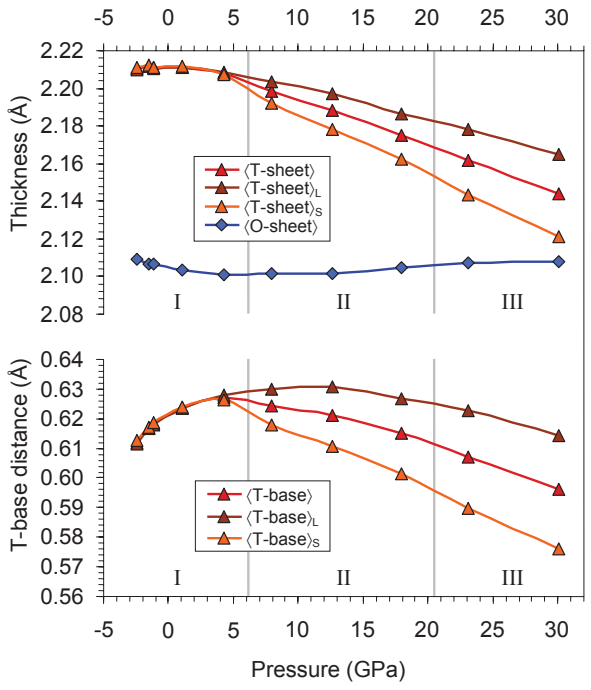

FIGURE 9. Average thickness of the T-sheet and O-sheet (**upper**) and average distance of the T-site from the tetrahedral base (**lower**) vs. pressure. The three pressure ranges individuated in this study are indicated (gray vertical lines). (Color online.)

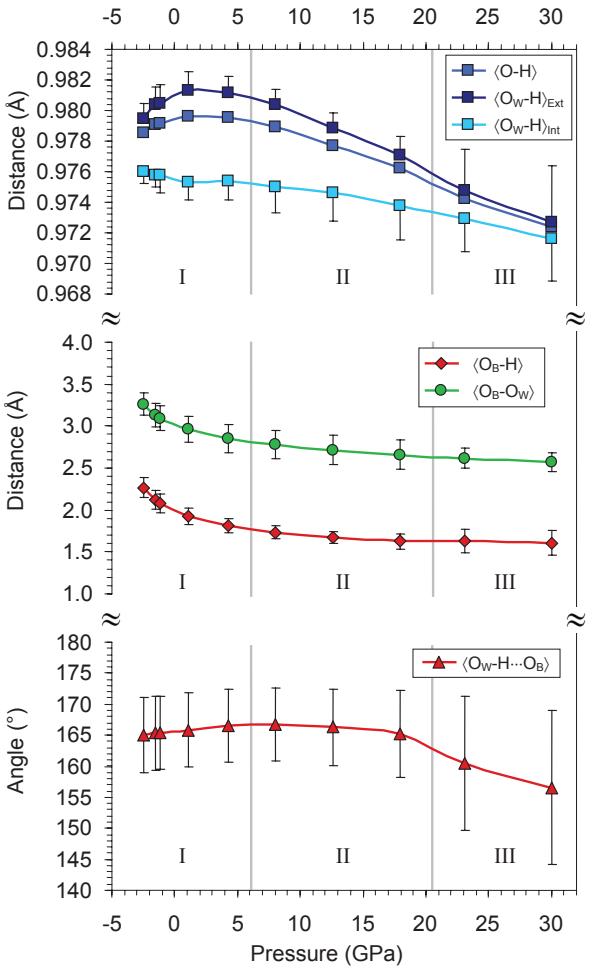

FIGURE 10. O-H bonding and angles vs. pressure for the m = 17 antigorite (OB = basal tetrahedral O atoms; OW = external octahedral O atoms). Bars indicate ranges of data dispersion around the average at one sigma level. (Color online.)

DISCUSSION AND CONCLUSIONS

Compression mechanism

Two major discontinuities affect the main structural parameters of antigorite upon compression, at about 6.1 GPa (unit-cell volume of 2650 Å^3), and at about 20.5 GPa (unit-cell volume of 2350 Å^3). These discontinuities allow the definition of three pressure ranges with different prevailing compression mechanisms:

(1) Low pressure. From negative pressure up to ~6 GPa, the *c*-axis is much more compressible than *a* and *b* and the unit-cell contraction is accomplished mostly by thinning of the interlayer. Compression in this regime is very similar to that in lizardite (Mellini and Zanazzi 1989; Auzende et al. 2006; Mookherjee and Stixrude 2009) and indeed in many sheet silicates including also talc (Stixrude 2002). In this pressure range, the MgO_6-octahedra compress more rapidly than the SiO_4-tetrahedra, permitting a better fit between the T-sheet and the O-sheet and increasingly ideal Mg-octahedra. The minimal mismatch occurs at the boundary of the low-pressure regime, i.e., at 6 GPa. The recovery of the geometrical mismatch between the T- and O-sheet upon compression leads to a change in the compression mechanism of other sheet silicates related to antigorite, such as lizardite (Mookherjee and Stixrude 2009) and talc (Stixrude 2002), and recently Mookherjee and Capitani (2011) have found a change in the elastic properties of antigorite at the point were the T- and the O- sheets record the minimal mismatch.

(2) Intermediate pressure. From ~6 GPa up to ~20 GPa, the ditrigonalization of the T-sheet becomes the dominant compression mechanism. In this pressure range, we also detect a gradual transition from flattening to bending. Compression affects the short and the long halfwaves at different rates. Structural parameters such as T-sheet thickness, Si-O bonds, 2α, and Si-O-Si angles assume distinct values for the short and long halfwaves, leading to symmetry breaking.

(3) Extreme pressure. From about 20 GPa onward, bending of the halfwaves takes over as the dominant compression mechanism. The O-H vectors angles become negative, paralleled by a quick decrease of the O_W-H···O_B angles; the *c* parameter and, especially, the *a* parameter soften.

We suggest that the softening encountered experimentally at 6 GPa by Nestola et al. (2009) has its origin in the transition in compression mechanism found theoretically at this same pressure. In the low-pressure range, interlayer thinning and wave flattening recover most of the geometrical mismatch between the T- and O-sheet. At the transition point, the differential compressibility of the tetrahedral and octahedral sheets vanishes, triggering a change toward different mechanisms, namely ditrigonalization of the T-sheet, to accommodate further contraction

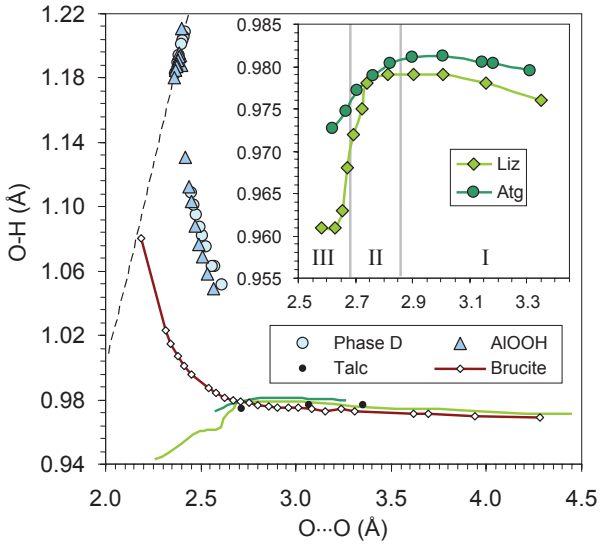

FIGURE 11. Plot of O-H bonds as a function of O···O distances for serpentine and other hydrated phases: talc (Stixrude 2002), δ-AlOOH (Panero and Stixrude 2004), phase D (Tsuchiya et al. 2005), and brucite (Mookherjee and Stixrude 2006); the dashed line depicts the condition for symmetric hydrogen bonding i.e., O···O = 2(O-H). Inset: details of the average O-H vs. interlayer O···O distances for antigorite and lizardite (Mookherjee and Stixrude 2009) in the pressure range investigated in this study (up to 30 GPa). The point where the two trends come closer is where lizardite experiences a structural transition at ~7 GPa. (Color online.)

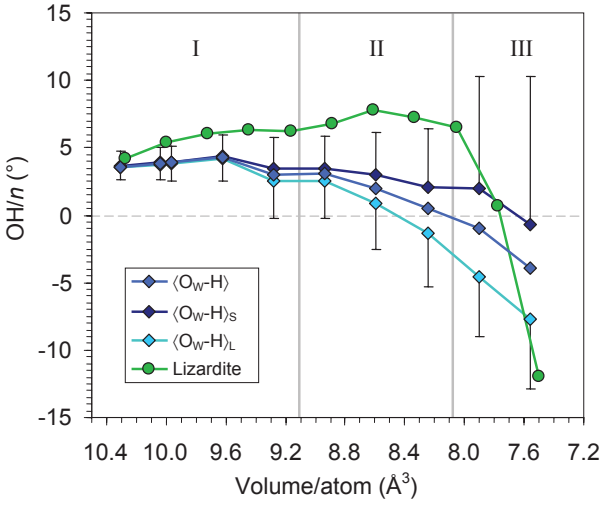

FIGURE 12. Average angle that O-H vectors of the external hydroxyls form with the (001) normal at the center of its ditrigon (OH/n) as function of volume/atom for antigorite (diamonds, L = long halfwave, S = short halfwave) and lizardite (circles, Mookherjee and Stixrude 2009). Bars indicate ranges of data dispersion around the average at one sigma level. (Color online.)

in the intermediate-pressure range.

Along the same line, the transition in compression mechanism is also the cause of the softening of some elastic constants found theoretically by Mookherjee and Capitani (2011). The relative magnitude and the trend upon compression of the C_{11}, C_{22}, and C_{33}, directly related to the compressibility along the **a**-, **b**-, and **c**-axis, respectively, are fully consistent with the linear compressibility found in this study. The softening of C_{11} and C_{22} is consistent with the transition in the compression mechanism described above. In the intermediate pressure range, the wave is no longer easily compressible along the stacking direction (C_{33} stiffens), and become comparatively more compressible through ditrigonalization and wave bending, which entail in-plane shortening (C_{11} and C_{22} soften).

Relative stability of serpentine polymorphs

The vanishing of the tetrahedral bulk modulus observed in lizardite in the 7–23 GPa pressure range and related to a change in interaction of the hydroxyls with the basal tetrahedral O atoms is not observed in antigorite. The lack of this mechanical instability in antigorite may explain the higher stability field of antigorite among the serpentine minerals (Evans et al. 1976; Bose and Ganguly 1995; Ulmer and Trommsdorff 1995; Wunder and Schreyer 1997). The cause of the lack of this mechanical instability is less palpable, but may be found in the slightly different O_W-H···O_B environment and its different evolution with pressure, as testified by the O_W-H···O_B angle and O-H angle evolution with pressure, and by the O-H vs. O···O diagram (Figs. 10 and 11). These in turn engender from the wavy nature of the structure and its peculiar compression mechanism.

One striking point of the observed response of the m = 17 ("odd") antigorite to compression is the significantly different behavior of the short halfwave as compared with the long one. The difference originates at ~6 GPa and concerns mainly the wave bending, the Si-O bonding, the T-sheet stretching and the H-bonding. One may wonder whether "even" antigorite polysomes with symmetrical halfwaves, as m = 16 (Capitani and Mellini 2006, 2007), may have different structural behavior under extreme compression. Along this line, one may wonder also whether different compression mechanisms could characterize even polysomes with odd number of tetrahedra in a halfwave and polysomes with an even number of tetrahedra in a halfwave (i.e., m = 14 or 18 vs. m = 16, respectively). The positive correlation of the polysome m number with pressure proposed by Wunder et al. (2001) and discarded by Hilairet et al. (2006b) on the base of the similarity of the compression behavior of lizardite, chrysotile, and antigorite, need to be re-examined.

Amorphization

The compression behavior of antigorite may shed light on the origin of intermediate depth earthquakes in subduction zones. One proposed mechanism is pressure-induced amorphization (Meade and Jeanloz 1991). Amorphization was found to occur in lizardite in a pressure interval between 6 and 22 GPa at room temperature, thus within the conditions investigated in this study. One recurrent structural parameter considered as an index of structural instability is the Si-O-Si angle (Stixrude 2002), considered critical below 122°, the smallest value found in silicates at ambient conditions (O'Keeffe and Hyde 1978), and achieved in our simulated structures over the pressure interval 22–28 GPa (Fig. 7). This result is consistent with X-ray diffraction experiments of Irifune et al. (1996), who did not find amorphization of antigorite at pressure up to 28 GPa at room temperature, and

with the IR spectroscopy experiments of Noguchi et al. (2012), who did not observe amorphization at pressure up to 25 GPa and temperatures up to 300 °C.

Amorphization was indeed detected by Noguchi et al. (2012) at 300 °C and 25.6 GPa through the appearance of a broad band resembling that of hydrous silicate glasses, and attributed to disordered OH groups. A sharp band at 3737 cm^{-1}, however, was also detected within the broad band, and attributed to the OH_{inner} stretching mode, demonstrating surviving short-range order around OH groups within the TO layer. It was concluded that disordered and relict OH groups were present within the amorphized antigorite structure. Our results offer an alternative interpretation of the IR spectrum. The rapid increase at pressures above 20 GPa of the range of OH structural parameters, namely of the O_W-H···O_B angles, O_W-H bond lengths, and orientations (Figs. 10 and 12), suggests that the large absorption band could be explained by a natural structural evolution of the crystal rather than by amorphization.

Corrugated vs. flat serpentines

Our theoretical results may contribute to shed light on the parameters that control the occurrence of corrugated structures in chrysotile and antigorite, which are still a matter of debate. One way of thinking is that merely geometrical lateral mismatch between the O- and T-sheets is the cause of the tubular habit of lizardite and of the wavy structure of antigorite (e.g., Wicks and O'Hanley 1988; Perbost et al. 2003). The lateral dimensions of an ideal trioctahedral sheet ($a \approx 5.4$; $b \approx 9.3$ Å) are somewhat greater than the lateral dimensions of an ideal tetrahedral sheet ($a \approx 5.0$; $b \approx 8.7$ Å), thus impeding a perfect T-O linkage. Through bending of the TO-layer and positioning the T-sheet internally, the distance between adjacent apical O atoms increases, whereas the distance between the internal octahedral O atoms decreases, allowing perfect T-O linkage. In lizardite, the flat serpentine polymorph, this corrugation does not occur. In most cases, the explanation that has been reported is that significant $^{IV}Al^{3+}$ (effective ionic radius 0.39 Å; Shannon 1976) enters the T-sites substituting for Si^{4+} (0.26 Å) and significant $^{VI}Al^{3+}$ (0.54 Å) enters the M-sites substituting for Mg^{2+} (0.72 Å), thus increasing the lateral dimension of the T-sheet and decreasing that of the O-sheet, eventually allowing a perfect T-O linkage.

An alternative way of thinking is that in the lizardite structure the coupled substitution of Si^{4+} and Mg^{2+} by trivalent cations such as Al^{3+} or Fe^{3+} is able to positively polarize the O-sheet and negatively polarize the T-sheet, thus promoting a stronger interlayer bonding and flat structures (Mellini 1982; Mellini and Zanazzi 1987; Mellini and Viti 1994).

A notable feature of serpentine minerals is the ditrigonal distortion of the tetrahedral sheet, usually invoked as a measure of the interlayer hydrogen bonding. According to the more reliable crystal-structure refinements, ditrigonal distortion is negative in lizardite-1*T* (Mellini 1982; Mellini and Zanazzi 1987; Mellini and Viti 1994; Mellini et al. 2010) and antigorite (Capitani and Mellini 2004, 2006), and positive in lizardite-2H_1 (Mellini and Zanazzi 1987) and alluminian lizardite-2H_2 (Brigatti et al. 1997). That seems related to the achievement of the best possible hydrogen bonding (Mellini 1982). It is noteworthy that the equilibrium structures of pure Mg end-members modeled by DFT theory have positive ditrigonal distortion in lizardite-1*T* (Mookherjee and Stixrude 2009) and negative ditrigonal distortion in antigorite (Capitani et al. 2009). This observation, along with the recurrent higher content of trivalent substituents observed in natural lizardite than in coexisting chrysotile and antigorite (Viti and Mellini 1996, 1997), probably suggests that substituents actually play a definite role in the corrugation of serpentine. The possible scenario is that: (1) Al-poor serpentine forms curled structures with negative ditrigonal distortion; (2) substituted serpentine forms flat structures with negative ditrigonal distortion; and (3) highly substituted serpentine forms flat structures with positive ditrigonal distortion. These would be the conditions to realize the best possible interlayer bonding.

Our theoretical results support this hypothesis. A comparison of the O-H bonds vs. the O···O bonds for antigorite and lizardite (Fig. 11) actually shows that the average O-H distances of antigorite, for a given interlayer separation, are systematically longer than those of lizardite along the pressure range investigated, i.e., antigorite is more efficiently bonded. The two trends come closer at the point where lizardite experiences a structural transition at about 7 GPa, afterward, for increasing compression, the difference increases drastically. This observation should suggest that in pure Mg-end-member serpentines a stronger hydrogen bonding is achievable with a wavy structure and a negative ditrigonal distortion than in a flat structure, and may also explain the greater stability field at high pressure of antigorite.

Unfortunately things do no seem to go so simply in nature, since lizardite structures with either negative or positive ditrigonal distortion and similar composition have been refined (Mellini and Zanazzi 1987); an almost pure Mg-lizardite with 1*T* structure has been recently refined (Mellini et al. 2010); and antigorite with significant Al-content has been recently reported (Padrón-Navarta et al. 2008). Additional factors other than composition, presumably growth factors, may contribute to the serpentine polymorphism and polytypism.

Acknowledgments

This work was possible thanks to a grant for computer time at the Caspur HPC facilities to GCC. Luca Ferraro is greatly acknowledged for computer help with the "Poseidon" AMD Opteron Cluster and Mainak Mookherjee for providing lizardite data and fruitful suggestions. Simon Redfern and an anonymous referee provided valuable revision of the manuscript.

References cited

Anderson, O.L. (1995) Equations of state of solids for geophysics and ceramic science. Oxford University Press, U.K.

Auzende, A., Daniel, I., Reynard, B., Lemaire, C., and Guyot, F. (2004) High-pressure behavior of serpentine minerals: a Raman spectroscopic study. Physics and Chemistry of Minerals, 31, 269–277.

Auzende, A., Pellenq, R.J.M., Devouard, B., Baronnet, A., and Grauby, O. (2006) Atomistic calculations of structural and elastic properties of serpentine minerals: the case of lizardite. Physics and Chemistry of Minerals, 33, 266–275.

Bezacier, L., Reynard, B., Bass, J.D., Sanchez-Valle, C., and Van de Moortele, B. (2010) Elasticity of antigorite, seismic detection of serpentinites, and anisotropy in subduction zones. Earth and Planetary Science Letters, 289, 198–208, DOI: 10.1016/j.epsl.2009.11.009.

Birch, F. (1947) Finite elastic strain of cubic crystals. Physical Review, 71, 809–824.

Bose, K. and Ganguly, J. (1995) Experimental and theoretical studies of the stabilities of talc, antigorite and phase A at high pressures with applications to subduction processes. Earth and Planetary Science Letters, 136, 109–121.

Brigatti, M.F., Galli, E., Medici, L., and Poppi, L. (1997) Crystal structure refinement of aluminian lizardite-2H_2. American Mineralogist, 82, 931–935.

Capitani, G.C. and Mellini, M. (2004) The modulated crystal structure of antigorite: the m = 17 polysome. American Mineralogist, 89, 147–158.

——— (2005) HRTEM evidence for 8-reversals in the $m = 17$ polysome. American Mineralogist, 90, 991–999.
——— (2006) The crystal structure of a second antigorite polysome ($m = 16$), by single crystal synchrotron diffraction. American Mineralogist, 91, 394–399.
——— (2007) High-resolution transmission electron microscopy (HRTEM) investigation of antigorite polysomes ($m = 15$ to 18). American Mineralogist, 92, 64–71.
Capitani, G.C., Stixrude, L., and Mellini, M. (2009) First-principles energetics and structural relaxation of antigorite. American Mineralogist, 94, 1271–1278.
Dobson, D.P., Meredith, P.G., and Boon, S.A. (2002) Simulation of subduction zone seismicity by dehydration of serpentine. Science, 298, 1407–1410.
Evans, B.W., Johannes, W., Oterdoom, H., and Trommsdorff, V. (1976) Stability of chrysotile and antigorite in the serpentine multisystem. Schweizer Mineralogische und Petrographische Mitteilungen, 56, 79–93.
Faust, J. and Knittle, E. (1994) The equation of state, amorphization, and high pressure phase-diagram of muscovite. Journal of Geophysical Research, 99, 19, 785–792.
Fumagalli, P. and Stixrude, L. (2007) The 10 Å phase at high pressure by first principles calculations and implications for the petrology of subduction zones. Earth and Planetary Science Letters, 260, 212–226.
Heine, V. (1970) The pseudopotential concept. Solid State Physics, 24, 1–37.
Hilairet, N., Daniel, I., and Reynard, B. (2006a) Equation of state of antigorite, stability field of serpentines, and seismicity in subduction zones. Geophysical Research Letters, 33, L02302.
Hilairet, N., Daniel, I., and Reynard, B. (2006b) P–V equations of state and the relative stabilities of serpentine. Physics and Chemistry of Minerals, 33, 629–637.
Ita, J.J. and Stixrude, L. (1992) Petrology, elasticity, and composition of the mantle transition zone, Journal of Geophysical Researches, 97, 6849–6866.
Irifune, T., Kuroda, K., Funamori, N., Uchida, T., Yagi, T., Inoue, T., and Miyajima, N. (1996) Amorphization of serpentine at high pressure and high temperature. Science, 272, 1468–1470.
Kresse, G. and Furthmüller, J. (1996a) Efficiency of *ab initio* total energy calculations for metals and semiconductors. Computational Material Science, 6, 15–50.
——— (1996b) Efficient iterative schemes for *ab initio* total energy calculations using a planewave basis set. Physical Review B, 54, 11169–11186.
Kresse, G. and Hafner, J. (1993) Ab initio molecular-dynamics for liquid-metals. Physical Review B, 47, 558–561.
Kresse, G., Hafner, J., and Needs, R.J. (1992) Optimized norm-conserving pseudopotentials. Journal of Physics-Condensed Matter, 4, 7451–7468.
Lundqvist, S. and March, N.H. (1983) Theory of the Inhomogeneous Electron Gas. Plenum, New York.
Meade, C. and Jeanloz, R. (1991) Deep-focus earthquakes and recycling of water into the earth's mantle. Science, 252, 68–72.
Mellini, M. (1982) The crystal structure of lizardite 1*T*: hydrogen bonding and polytypism. American Mineralogist, 67, 587–598.
Mellini, M., Cressey, G., Wicks, F.J., and Cressey, B.A. (2010) The crystal structure of Mg end-member lizardite-1*T* forming polyhedral spheres from the Lizard, Cornwall. Mineralogical Magazine, 74, 277–284.
Mellini, M. and Viti, C. (1994) Crystal structure of lizardite-1*T* from Elba, Italy. American Mineralogist, 79, 1194–1198.
Mellini, M. and Zanazzi, P.F. (1987) Crystal structure of lizardite-1*T* and lizardite-2H_1 from Coli, Italy. American Mineralogist, 72, 943–948.
——— (1989) Effects of pressure on the structure of lizardite-1*T*. European Journal of Mineralogy, 1, 13–19.
Monkhorst, H.J. and Pack, J.D. (1976) Special points for Brillouin-zone integrations. Physical Review B, 13, 5188–5192.
Mookherjee, M. and Capitani, G.C. (2011) Elasticity and anisotropy of antigorite at high pressure, Geophysical Research Letters, 38, L09315, DOI: 10.1029/2011GL047160.
Mookherjee, M. and Stixrude, L. (2006) High-pressure proton disorder in brucite. American Mineralogist, 91, 127–134.
——— (2009) Structure and elasticity of serpentine at high-pressure. Earth and Planetary Science Letters, 279, 11–19.
Nestola, F., Angel, J.R., Zhao, J., Garrido, C.J., López Sánchez-Vizcaíno, V., Capitani, G.C., and Mellini, M. (2009) Antigorite equation of state and anomalous softening at 6 GPa: An in-situ single-crystal X-ray diffraction study. Contributions to Mineralogy and Petrology, 160, 33–43, DOI: 10.1007/s00410-009-0463-9.
Noguchi, N., Moriwaky, T., Ikemoto, Y., and Shinoda, K. (2012) OH group behavior and pressure-induced amorphization of antigorite examined by high pressure and temperature using synchrotron infrared spectroscopy. American Mineralogist, 97, 134–142.
O'Keeffe, M. and Hyde, B.G. (1978) On Si-O-Si configurations in silicates, Acta Crystallographica, B34, 27–32.
Padrón-Navarta, J.A., López Sánchez-Vizcaíno, V., Garrido, C.J., Gómez Pugnaire, M.T., Jabaloy, A., Capitani, G.C., and Mellini, M. (2008) Highly ordered antigorite from Cerro del Almirez HP-HT serpentinites, SE Spain. Contributions to Mineralogy and Petrology, 156, 679–688.
Panero, W.R. and Stixrude, L. (2004) Hydrogen incorporation in stishovite at high pressure and symmetric hydrogen bonding in δ-AlOOH. Earth and Planetary Science Letters, 221, 421–431.
Peacock, S.M. (2001) Are the lower planes of double seismic zones caused by serpentine dehydration in subducting oceanic mantle? Geology, 29, 299–302.
Perbost, R., Amouric, M., and Olives, J. (2003) Influence of cation size on the curvature of serpentine minerals: HRTEM-AEM study and elastic theory. Clay and Clay Minerals, 51, 430–438.
Perdew, J.P., Burke, K., and Ernzerhof, M. (1996) Generalized gradient approximation made simple. Physical Review Letters, 77, 3865–3868.
Reynard, B. and Wunder, B. (2006) High-pressure behavior of synthetic antigorite in the Mgo-SiO_2-H_2O system from Raman spectroscopy. American Mineralogist, 91, 459–462.
Robinson, K., Gibbs, G.V., and Ribbe, P.H. (1971) Quadratic elongation: A quantitative measure of distortion in coordination polyhedra. Science, 172, 567–570.
Shannon, R.D. (1976) Revised effective ionic radii and systematic studies of interatomic distances in halides and chalcogenides. Acta Crystallographica. A32, 751–767.
Stixrude, L. (2002) Talc under tension and compression: Spinodal instability, elasticity, and structure. Journal of Geophysical Research, 107, 23–27.
Tonarini, S., Agostini, S., Doglioni, C., Innocenti, F., and Manetti, P. (2007) Evidence for serpentinite fluid in convergent margin systems: The example of El Salvador (Central America) arc lavas. Geochemistry, Geophysics, Geosystems, 8, Q09014, DOI: 10.1029/2006GC001508.
Tsuchiya, J., Tsuchiya, T., and Suneyuki, S. (2005) First-principle study of hydrogen bond symmetrization of phase D under high pressure. American Mineralogist, 90, 44–49.
Uehara, S. and Shirozu, H. (1985) Variations in chemical composition and structural properties of antigorites. Mineralogical Journal, 12, 299–318.
Ulmer, P. and Trommsdorff, V. (1995) Serpentine stability to mantle depths and subduction related magmatism. Science, 268, 858–861.
Vanderbilt, D. (1990) Soft self-consistent pseudopotentials in a generalized eigenvalue formalism. Physical Review B, 41, 7892–7895.
Viti, C. and Mellini, M. (1996) Vein antigorites from Elba Island, Italy. European Journal of Mineralogy, 8, 423–434.
——— (1997) Contrasting chemical compositions in associated lizardite and chrysotile in veins from Elba, Italy. European Journal of Mineralogy, 9, 585–596.
Wentzcovitch, R.M. (1991) Invariant molecular dynamics approach to structural phase transitions. Physical Review B, 44, 2358–2361.
Wentzcovitch, R.M. and Stixrude, L. (1997) Crystal chemistry of forsterite: A first-principle study. American Mineralogist, 82, 663–671.
Wentzcovitch, R.M., Martins, J.L., and Price, G.D. (1993) Ab initio molecular dynamics with variable cell shape: application to $MgSiO_3$ perovskite. Physical Review Letters, 70, 3947–3950.
Wicks, F.J. and O'Hanley, D. (1988) Serpentine minerals: structure and petrology. In Bailey, S.W., Ed., Hydrous Phyllosilicates, 19, p. 91–167. Reviews in Mineralogy, Mineralogical Society of America, Chantilly, Virginia.
Wunder, B. and Schreyer, W. (1997) Antigorite: High-pressure stability in the system MgO-SiO_2-H_2O (MSH). Lithos, 41, 213–227.
Wunder, B., Wirth, R., and Gottschalk, M. (2001) Antigorite: Pressure and temperature dependence of polysomatism and water content. European Journal of Mineralogy, 13, 485–495.
Yamasaki, T. and Seno, T. (2003) Double seismic zone and dehydration embrittlement of the subducting slab. Journal of Geophysical Research, 108, 2212.

Manuscript received July 19, 2011
Manuscript accepted March 25, 2012
Manuscript handled by Simon Redfern